Optimizing Interface Conductivity in Electronics

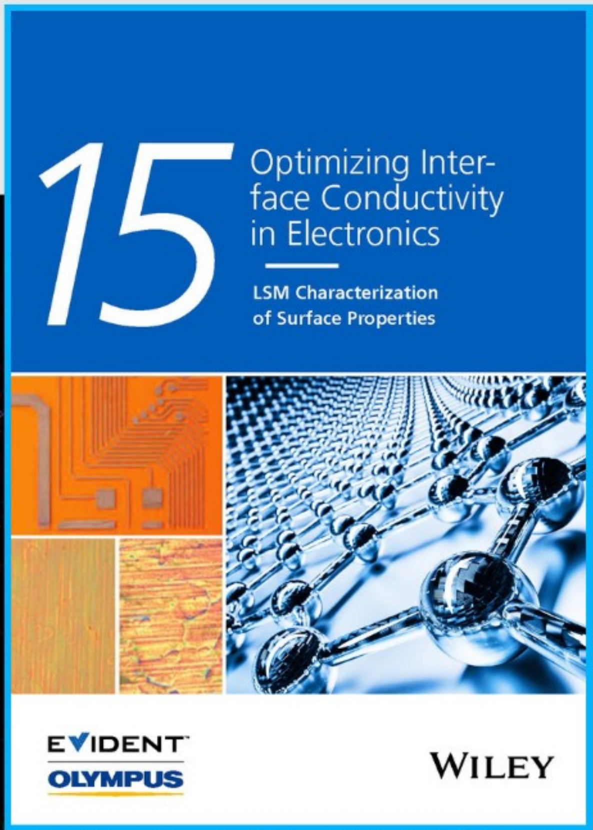

The latest eBook from Advanced Optical Metrology. Download for free.

Surface roughness is a key parameter for judging the performance of a given material's surface quality for its electronic application. A powerful tool to measure surface roughness is 3D laser scanning confocal microscopy (LSM), which will allow you to assess roughness and compare production and finishing methods, and improve these methods based on mathematical models.

Focus on creating high-conductivity electronic devices with minimal power loss using laser scanning microscopy is an effective tool to discern a variety of roughness parameters.

Fluorinated Pentafulvalene-Fused Hole-Transporting Material Enhances the Performance of Perovskite Solar Cells with Efficiency Exceeding 23%

*Kun-Mu Lee, Yao-Shen Huang, Wei-Hao Chiu, Ying-Kai Huang, Gao Chen, Gizachew Belay Adugna, Sie-Rong Li, Fang-Ju Lin, Shih-I. Lu, Hsiao-Chi Hsieh, Kang-Ling Liau, Chun-Cheng Huang, Yian Tai, Yu-Tai Tao, and Yan-Duo Lin**

Organic small molecular materials with coplanar π-conjugated system as HTMs in perovskite solar cells (PSCs) have attracted considerable attention due to their high charge transport capability and thermal stability. Herein, three novel pentafulvalene-fused derivatives with or without fluorine atoms incorporated (YSH-*o*F and YSH-*m*F and YSH-H, respectively) are designed, synthesized, and applied as hole-transporting materials (HTMs) in PSCs fabrication. The fluorinated HTMs, YSH-*o*F and YSH-*m*F, exhibited higher hole mobility and better charge extraction at the perovskite/HTM interface than non-fluorinated one do, presumably due to the closer intermolecular π–π packing interactions. As a result, small-area (0.09 cm^2) PSCs made with YSH-*o*F and YSH-*m*F achieved an impressive power conversion efficiency (PCE) of 23.59% and 22.76% respectively, with negligible hysteresis, in contrast with the 20.57% for the YSH-H-based devices. Furthermore, for large-area (1.00 cm^2) devices, the PSCs employing YSH-*o*F exhibited a PCE of 21.92%. Moreover, excellent long-term device stability is demonstrated for PSCs with F-substituted HTMs (YSH-*o*F and YSH-*m*F), presumably due to the higher hydrophobicity. This study shows the great potential of fluorinated pentafulvalene-fused materials as low-cost HTM for efficient and stable PSCs.

1. Introduction

Perovskite solar cells (PSCs) have received a great deal of attention and have gone through rapid development in the past decade because of their advantages of strong light-harvesting capability, low-cost assembling techniques, and outstanding power conversion efficiency (PCE).[1] At present, the certified record PCE over 25% has been achieved in state-of-the-art PSCs, which is comparable with that of commercial crystalline silicon solar cells. PSCs based on sandwich-like structure with the hole transport layer and the electron transport layer have afforded high PCE.[2] Among the factors that affect the PCE, the hole transport material (HTM) plays a key role, as it is closely related to PCE as well as device stability.[3] To date, 2,2′,7,7′-tetrakis-(*N*,*N*-di-*p*-methoxyphenylamine)−9,9′-spirobifluorene (spiro-OMeTAD) is the most widely used HTM for n-i-p device

K.-M. Lee, W.-H. Chiu, Y.-K. Huang
Department of Chemical and Materials Engineering
Chang Gung University
Taoyuan 33302, Taiwan

K.-M. Lee
Division of Neonatology
Department of Pediatrics
Chang Gung Memorial Hospital
Linkou, Taoyuan 33305, Taiwan

K.-M. Lee, W.-H. Chiu
Center for Green Technology
Chang Gung University
Taoyuan 33302, Taiwan

Y.-S. Huang, G. B. Adugna, S.-I. Lu, C.-C. Huang, Y.-D. Lin
Department of Chemistry
Soochow University
Taipei 11102, Taiwan
E-mail: ydlin@scu.edu.tw

The ORCID identification number(s) for the author(s) of this article can be found under https://doi.org/10.1002/adfm.202306367

DOI: 10.1002/adfm.202306367

G. Chen
Department of Applied Physics
The Hong Kong Polytechnic University
Hung Hom Kowloon
Hong Kong 999077, P. R. China

G. B. Adugna, S.-R. Li, F.-J. Lin, Y.-T. Tao
Institute of Chemistry
Academia Sinica
Taipei 115024, Taiwan

H.-C. Hsieh
Department of Applied Materials Science and Technology
Minghsin University of Science and Technology
Hsinchu 30401, Taiwan

K.-L. Liau
Department of Chemistry
National Central University
Taoyuan 32001, Taiwan

Y. Tai
Department of Chemical Engineering
National Taiwan University of Science and Technology
Taipei 10607, Taiwan

configuration, with a promising PCE over 20%.[4] Although its 3D structure can improve the solubility of the molecule and confer a uniform film, spiro-OMeTAD suffers from low intrinsic hole mobility owning to the weak intermolecular electronic coupling. Thus dopants (such as 4-*tert*-butylpyridine (*t*-BP) and lithium bis(trifluoromethanesulfonyl)imide (Li-TFSI)) are usually necessary to improve its conductivity and performance.[5] However, these additives cause instability of the film morphology of the HTM resulting from ionic migration, thus a dramatically drop in T_g under thermal stress. In addition, the complicated synthetic routes and purification process of spiro-OMeTAD increase the device fabrication cost, and thus inhibit the large-scale productions for commercialization. Consequently, the development of alternative HTMs with facile synthetic routes and thermal stability in the presence of additives while still maintaining high-performance PSCs is in great demand.

To get stable HTMs for PSCs, one possible strategy is to incorporate electron-withdrawing group (EWG) on the conjugated molecule. The HTMs with EWG substituent may have lower oxidation potential and thus improved thermal/photo-stability. Moreover, the down-shifted HOMO energy level could improve the open-circuit voltage (V_{oc}) values of PSCs and thus photovoltaic performance.[6] Among various types of organic conjugated molecule with strong electron-withdrawing capability, fluorinated derivatives have been made and used as HTMs in PSCs and showed improved hole mobility and conductivity by promoting intermolecular π–π interactions.[7] Meanwhile, the fluorinated HTMs could give rise to improved long-term stability of the PSCs owning to excellent water-resistance ability. However, until now only few fluorinated small-molecule HTMs have been developed for PSCs.[8]

Fused-thiophene conjugated molecules are of great interest as potential functional materials in electronic device because of their promising optoelectronic properties and high charge-carrier mobility. As a consequence, numerous HTMs molecules with fused-thiophene-based electron-rich building blocks have been developed and demonstrated to give high-performance PSCs, such as dithienothiophene (DTT), benzo[1,2-b:4,5-b′]dithiophene (BDT), benzo[1,2-b:3,4-b′:5,6-b′′]trithiophene (BTT), and other oligothiophenes.[9] Among thiophene-containing fused polycyclic scaffolds, cyclopenta[2,1-b:3,4-b’]dithiophene (CPDT) derivatives have been explored as HTMs owning to greater planarity and longer π-conjugation, facilitating intermolecular π–π packing interactions in the solid state, as well as the electron-donating ability of thiophene moiety.[10] Recently, we demonstrated that various core units of small CPDT-based molecules with different shapes including spiro-, donor-π-donor- (D-π-D), and donor-acceptor-donor-type (D-A-D) have been developed to give high-performance PSCs, exhibiting PCEs in the range of 17.59%–21.67%. This suggests that π-framework with CPDT moiety is a potential core for realizing high-performance HTMs.[11]

Pentafulvalene is a π-conjugated hydrocarbon composed of two cyclopentadiene rings connected by a cross-conjugated C═C double bond, which renders itself increased molecular planarity and rigidity and thus enhances intermolecular π–π interactions with improved charge carrier mobilities.[12] However, pentafulvalene is thermally unstable. Pentafulvalenes fused with arene groups have improved stability, such as 9,9′-bifluorenylidene (**99′BF**) and $\Delta^{4,4'}$-dicyclopenta[2,1-b:3,4-b′]-dithiophene (**DCDPT**) derivatives, where peripheral polycycles are introduced.[13] Furthermore, arene-fused pentafulvalene derivatives in general exhibit high electron-accepting property, which can make them electron-accepting π-conjugated materials. For example, Wudl and co-workers first proposed the small-molecule acceptor based on a **99′BF** backbone to replace fullerene acceptors for organic photovoltaics (OPVs) in 2010.[13a] On the other hand, Chi and co-workers reported the use of thiophene units to extend the conjugation of a DCDPT-based oligothiophenes as low band gaps materials in 2010.[14] However, Nazeeruddin et al. first reported that a 4,4′-dimethoxydiphenylamine-substituted 9,9′-bifluorenylidene-based material, coded as **KR216**, could also be applied as a HTM in PSCs, and achieved a PCE as high as 17.8% in 2016.[15] It has been demonstrated that arene-fused pentafulvalene molecules are the promising π-conjugated core structure for the development of charge transport materials, especially HTMs. Nevertheless, to our best knowledge, the material with DCDPT as core structure for PSCs have never been reported to date.

In this work, the three H-shaped pentafulvalene-fused HTMs (**YSH-*o*F**, **YSH-*m*F**, and **YSH-H**) comprising a $\Delta^{4,4'}$-dicyclopenta[2,1-b:3,4-b′]-dithiophene core with four arms of fluorinated triarylamine moieties (**YSH-*o*F** and **YSH-*m*F**) and non-fluorinated analogue (**YSH-H**) were rationally designed and synthesized (**Figure 1**). It is contemplated that these compounds combine the advantages of facilitated delocalization of π-conjugation and extended molecular conjugation to ensure high charge carrier mobility. Moreover, the perovskite defects could be passivated through interaction between sulfur and/or fluorine atoms in HTMs with uncoordinated Pb^{2+} or Pb clusters in the perovskite layer, as verified by X-ray photoelectron spectra (XPS) measurements. This can inhibit non-radiative recombination that can improve V_{oc} and photovoltaic performance.[16] According to the X-ray scattering (GIWAXS) measurements, it is found that **YSH-*o*F** exhibits closer packing and thus higher hole mobility relative to **YSH-*m*F**, and **YSH-H**. As a result, PSCs based on **YSH-*o*F** afford an excellent PCE of 23.59% for small-area (0.09 cm^2) devices with negligible hysteresis. In addition, **YSH-*o*F**-based PSC also exhibits a remarkable PCE of 21.92% for large-area (1.0 cm^2) device. Furthermore, the un-encapsulated devices with F-based HTMs, **YSH-*o*F** and **YSH-*m*F**, exhibited a better device stability than that of the non-fluorinated counterpart **YSH-H** and spiro-OMeTAD under various testing conditions such as ambient air at 20–25 °C, heated at 85 °C, and continuous light soaking. This could be attributed to the superior hydrophobicity and the smooth films in PSCs devices. Moreover, our synthetic costs of **YSH-*o*F**, **YSH-*m*F**, and **YSH-H** are estimated to be $92.16, $92.26, and $ 27.43 g^{-1}, respectively, which are much cheaper than that of spiro-OMeTAD (Tables S1–S13, Supporting Information). These results demonstrated the great potential of $\Delta^{4,4'}$-dicyclopenta[2,1-b:3,4-b′]-dithiophene-fused ring as a central π-framework in designing HTMs for high performance PSCs (.

2. Results and Discussion

The synthetic routes to prepare **YSH-*o*F**, **YSH-*m*F**, and **YSH-H** are shown in **Scheme 1**, and the experimental details including

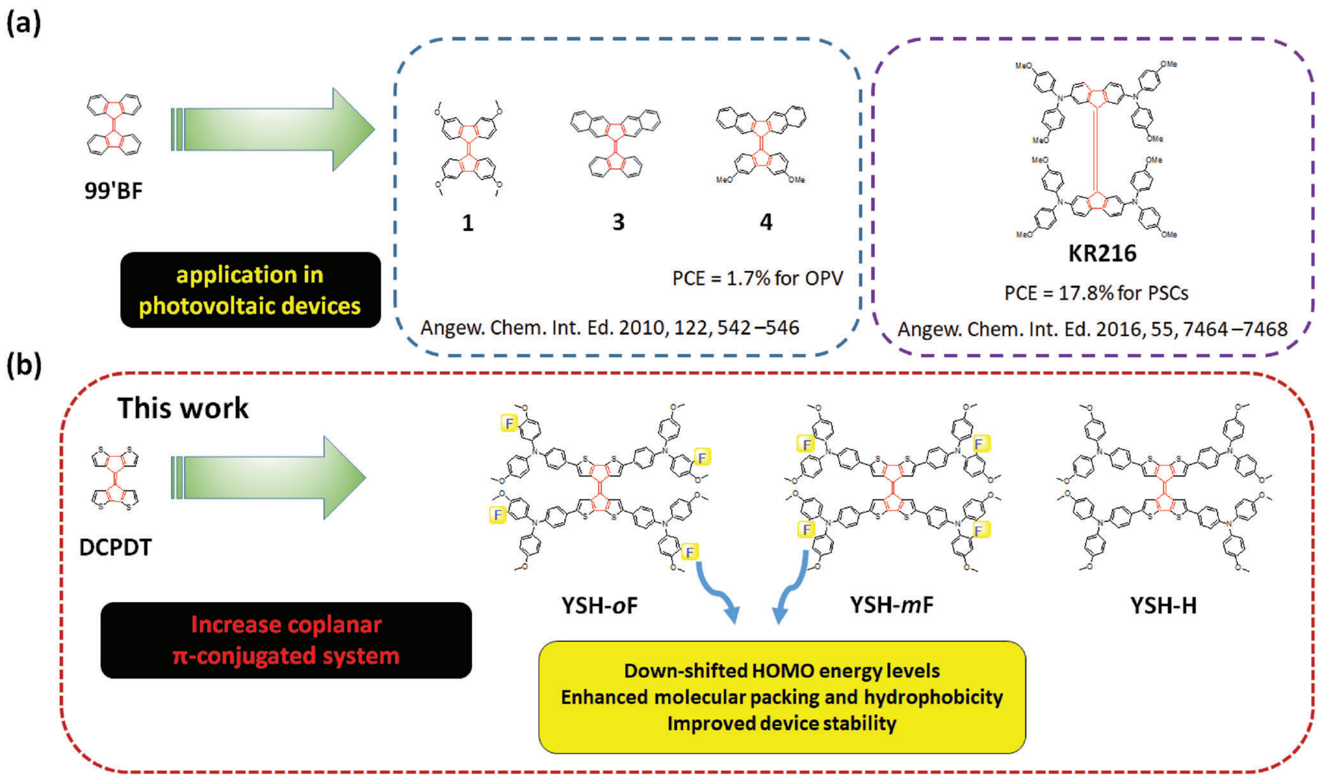

Figure 1. a) Chemical structures of the 9,9′-bifluorenylidene-based derivatives, b) molecular design concept and chemical structures of **YSH-*o*F**, **YSH-*m*F**, and **YSH-H**.

^{1}H NMR spectra, ^{13}C NMR spectra, ^{19}F NMR spectra and HRMS are provided in the Figures S1–S27 (Supporting Information). Compounds **3** and **4** were prepared by Buchwald−Hartwig coupling reaction of 1-bromo-4-iodobenzene with the known compounds **1** and **2**,[1d] respectively, and followed by reacting with bis(pinacol)borane in the presence of $PdCl_2(PPh_3)_2$ and KOAc in a refluxing toluene solution to give **5** and **6**. Finally, the target compounds **YSH-*o*F**, **YSH-*m*F**, and **YSH-H** were successfully synthesized in high yields by four-fold Suzuki coupling reaction between tetrabromo-$\Delta^{4,4'}$-dicyclopenta[2,1-*b*:3,4-*b*′]dithiophene (**8**),[17] and **5**, **6**, and **7**[11a] respectively, using $Pd(PPh_3)_4$ as the catalyst. The laboratory synthesis cost analysis for the new HTMs were evaluated. As shown in Tables S1–S13 (Supporting Information), the estimated costs of **YSH-*o*F**, **YSH-*m*F**, and **YSH-H** are \$92.16, \$92.26, and \$ 27.43 g^{-1}, respectively, which are much cheaper than that of spiro-OMeTAD (\$170–475 g^{-1}).[18]

The thermal behaviors of **YSH-*o*F**, **YSH-*m*F**, and **YSH-H** were scrutinized by differential scanning calorimetry (DSC) and thermogravimetric analysis (TGA) measurements (Figure S28, Supporting Information), while the corresponding data summarized in **Table 1**. The decomposition temperatures (T_d, the temperature with 5% weight-loss) of the **YSH-*o*F**, **YSH-*m*F**, and **YSH-H** were measured to be 423, 400, and 431 °C, respectively, which indicate that the new HTMs are thermally stable for conventional device fabrication. The glass transition temperatures (T_g) for **YSH-*o*F**, **YSH-*m*F**, and **YSH-H** are 180, 179, 169 °C, respectively, which are higher than that of spiro-OMeTAD (125 °C), implying that **YSH-*o*F**, **YSH-*m*F**, and **YSH-H** tend to remain amorphous film upon operation, which is required feature for a long-lived device. Moreover, the powder X-ray diffraction (PXRD) was employed to investigate the crystallinity of **YSH-*o*F**, **YSH-*m*F**, and **YSH-H** films (Figure S29, Supporting Information). The target compounds exist in an amorphous state based on PXRD analysis, indicating that **YSH**-based HTMs are hard to crystalize, which in turn can enhance device long term stability.

The optimized geometries and electronic structures of **YSH-*o*F**, **YSH-*m*F**, and **YSH-H** were elucidated by density functional theory (DFT) calculations at B3LYP/6-31G (d,p) level. As illustrated in **Figure 2**a, the optimized molecular geometries of **YSH** series show the quasi-coplanar shape due to the repulsive steric hindrance between the hydrogens on the thiophene rings. The dihedral angles between the two double-bond connected CPDT are measured to be ≈23°. From the structural point of view, the increased rigidity and near planar structure of **YSH** series will be expected to enhance the intermolecular π–π interactions, which is beneficial to hole transport. Furthermore, DFT calculations were carried out to gain insight in the electron distribution of the frontier orbitals of the three molecules. As shown in Figure S30 (Supporting Information), the HOMOs are mostly localized on the two quasi-parallel CPDT along with the triphenylamine moieties, while the LUMOs were principally localized on the central backbone, indicating an intramolecular charge transfer (ICT) character may exist for the new HTMs. The HOMO and LUMO energy levels of **YSH-*o*F**, **YSH-*m*F**, and **YSH-H** were also evaluated by DFT calculations. The HOMO/LUMO are −4.50/−2.52, −4.31/−2.33, and −4.30/−2.39 eV for **YSH-*o*F**, **YSH-*m*F**, and **YSH-H**, respectively (Figure S30, Supporting Information). As

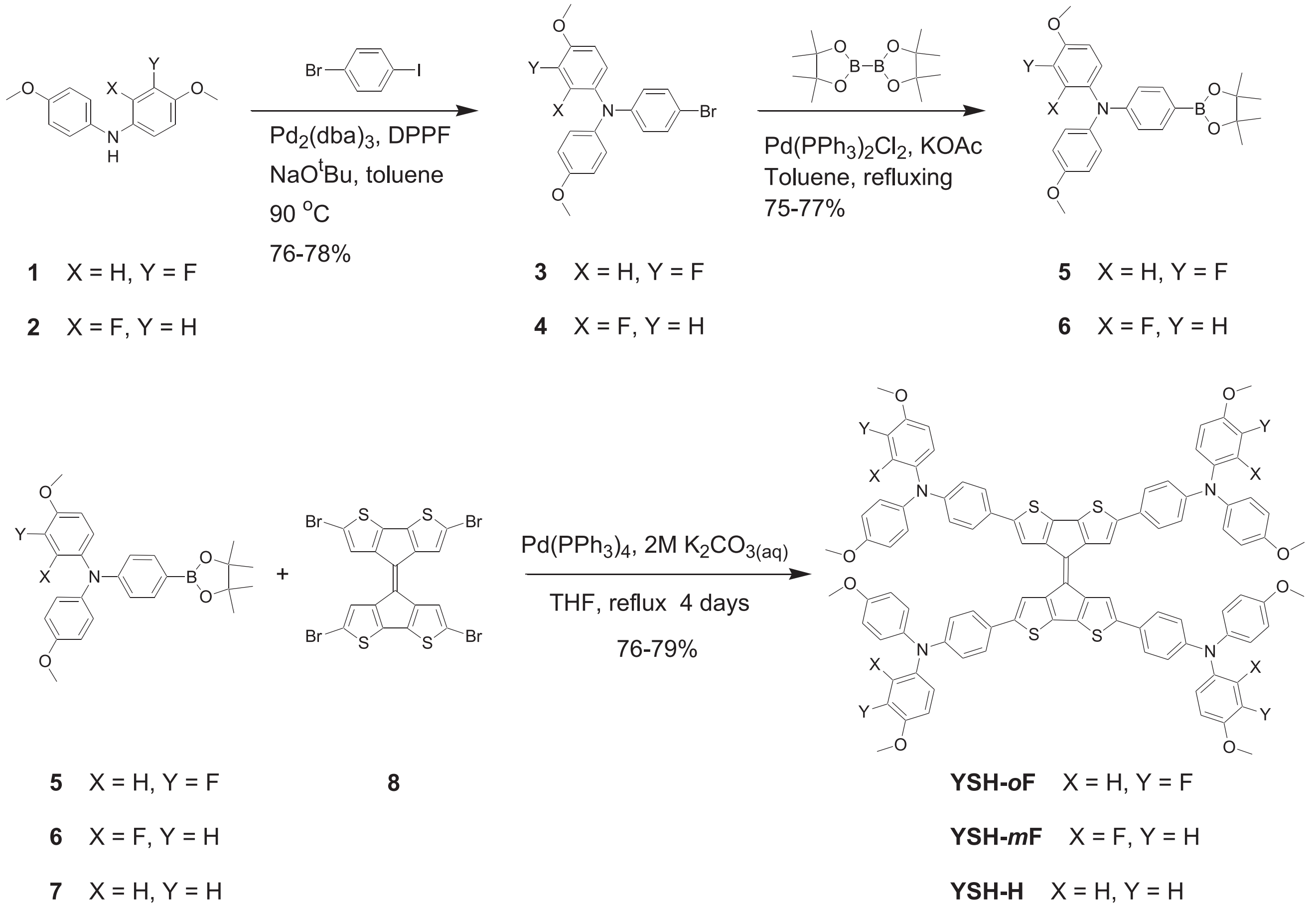

Scheme 1. Synthetic procedures for **YSH-*o*F**, **YSH-*m*F**, and **YSH-H**.

anticipated, fluorinated **YSH-*o*F** and **YSH-*m*F** have lower HOMO levels with respect to their non-fluorinated analogue (**YSH-H**) due to the electron-withdrawing character of fluorine atoms, which is beneficial to achieve a high open-circuit voltage (V_{oc}). Moreover, the dipole moment data of the **YSH** series is estimated by DFT calculations. Compared with **YSH-H** (1.38 D), **YSH-*o*F** and **YSH-*m*F** exhibit larger dipole moments of 4.83 and 4.44 D, respectively. The higher dipole moment of fluorinated HTMs may induce an enhanced dipole–dipole interaction, which could result in better charge transport and collection, which in turn lead to a higher J_{sc} and thus better overall efficiency.

The UV–vis absorption spectra of **YSH-*o*F**, **YSH-*m*F**, and **YSH-H** in THF solutions are shown in Figure 2b, while the corresponding parameters are listed in Table 1. The three HTMs exhibited similar absorption features with two strong absorption bands in the range of 250–500 nm, corresponding to the π–π* transition of the conjugated system, while the weak broad absorption peaks between 500 and 950 nm with absorption maximum at 690 nm are attributed to the intramolecular charge transfer (ICT) transitions from the TPA-CPDT-TPA segment to central pentafulvalene moiety, as suggested by DFT calculation. In addition, the fluorinated HTMs (**YSH-oF** and **YSH-*m*F**) show a slightly

Table 1. Photophysical, electrochemical and thermal data of **YSH-*o*F**, **YSH-*m*F**, **YSH-H** and spiro-OMeTAD.

HTM	λ_{abs} [nm] [$\epsilon \times 10^{-4}$/M^{-1} cm^{-1}] a)	E_{HOMO} [eV] b)	E_{0-0} [eV] c)	E_{LUMO} [eV] d)	E_{HOMO} [eV] e)	E_{0-0} [eV] e)	E_{LUMO} [eV] e)	T_g [°C] f)	T_d [°C] f)
YSH-*o*F	409 (13.9)	−5.19	1.31	−3.88	−4.45	1.83	−2.62	180	423
YSH-*m*F	404 (12.7)	−5.18	1.33	−3.85	−4.34	1.92	−2.42	179	400
YSH-H	412 (11.6)	−5.15	1.32	−3.83	−4.30	1.89	−2.41	169	431
spiro-OMTAD	389 (18.4)	−5.15	3.02	−2.13	−4.21	3.60	−0.61	121 g)	422 g)

a) Maxima of the absorption bands in THF solution; b) Determined by differential pulse voltammetry (DPV); c) The value of E_{0-0} obtained from the onset of absorption spectra; d) Energy of the LUMO of the compounds estimated by $E_{HOMO}+E_{0-0}$.; e) Values calculated at DFT/B3LYP/6-31G(d,p) level; f) Glass transition (T_g) and decomposition (T_d) temperatures observed from TGA and DSC, respectively; g) These dates have been reported in reference [6].

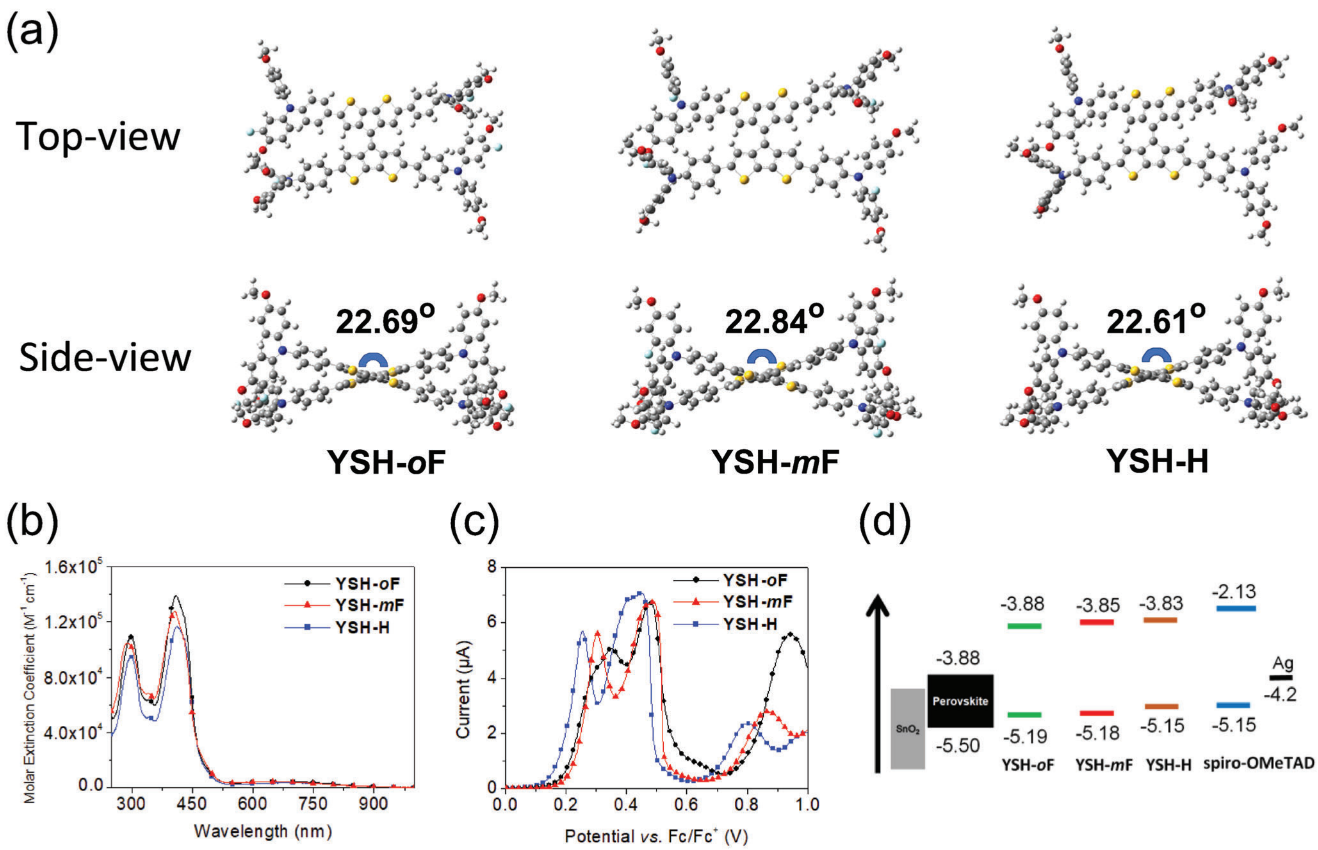

Figure 2. a) Top view and side view of the optimized structures for **YSH** series obtained from DFT calculations. b) Absorption spectra of **YSH** series in THF solution. c) Differential pulsed voltammetry (DPV) curves of **YSH** series in THF solution. d) Energy level alignment diagram of PSCs with **YSH-*o*F**, **YSH-*m*F**, **YSH-H** and spiro-OMeTAD as the HTM.

blue-shifted absorption maxima compared with non-fluorinated one at ≈410 nm, which may be attributed to the electron-withdrawing inductive effect of the fluorine atoms on the aromatic ring.[7a] The optical energy band gap (E_g) of HTMs was calculated to be 1.31 eV for **YSH-*o*F**, 1.33 eV for **YSH-*m*F**, and 1.32 eV for **YSH-H**, respectively from the absorption edges. Furthermore, the time-dependent density functional theory (TDDFT) method was performed to provide insights into the simulated absorption spectra, excitation energies (E_{ex}), and oscillator strengths (f) of the **YSH** series. The calculated UV−vis spectra are shown in Figure S31 (Supporting Information). The TDDFT excited states calculations were performed on the lowest 12 singlet–singlet excitations of **YSH-*o*F**, **YSH-*m*F**, and **YSH-H**, neglecting the influence of solvent. The theoretical E_{ex}, f values, and absorption wavelengths (λ_{max}) are listed in Tables S14–S16 (Supporting Information). According to TDDFT calculations at the B3LYP/6-31G (d,p) level of theory, the two main absorption bands of **YSH** series at short wavelength region (350–470 nm) can be attributed to the localized π–π* electronic transition of the polycyclic conjugated system, while the absorption band in the long wavelength region with the low absorption intensity (f = 0.0125–0.0364) at ≈840–860 nm should be ascribed to the ICT character, corresponding to HOMO → LUMO transition. The shape of simulated UV–vis spectra for **YSH-*o*F**, **YSH-*m*F**, and **YSH-H** is consistent with the experimental results as shown in Figure 2b. The TDDFT calculations have provided a theoretical support of our experimental spectral characteristics.

To gain insight into the redox properties of **YSH** series, the differential pulse voltammetry (DPV) measurements were conducted in THF solution, and the detailed electrochemical data are shown in Table 1. As shown in Figure 2c, the HOMO energy levels of **YSH-*o*F**, **YSH-*m*F**, and **YSH-H** are calculated to be −5.19, −5.18, and −5.15 eV, respectively, which are more positive compared to perovskite valence band (−5.50 eV), indicating that the photogenerated hole can easily transfer from perovskite to HTM layer. Moreover, the introduction of fluorine atom in **YSH-*o*F** and **YSH-*m*F** leads to deeper HOMO energy levels in comparison with that of **YSH-H** due to the strong electronegativity of fluorine, making them more compatible with the valence band of perovskite and thus more favorable for suppressing voltage loss and achieving a high V_{oc} of the solar cell. The LUMO energy level of **YSH-*o*F**, **YSH-*m*F**, and **YSH-H** can be deduced from E_{HOMO} and E_g to give −3.88, −3.85, and 3.83 eV, respectively, suggesting there will be efficient blocking of the reverse electron transfer from the perovskite conduction band to metal counter electrode (Figure 2d). The experimental measured HOMO and LUMO levels are in good consistency with the similar trend of DFT calculations (Figure S30, Supporting Information).

The hole-transport properties of **YSH-*o*F**, **YSH-*m*F**, and **YSH-H** were evaluated by the space-charge-limited current

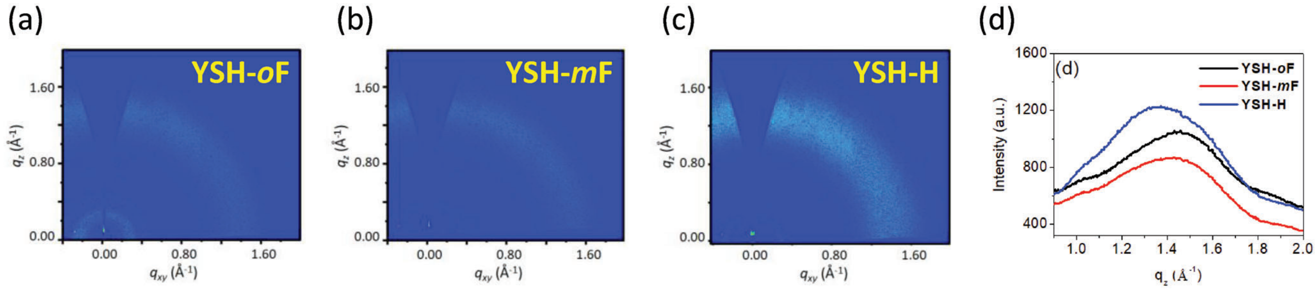

Figure 3. The GIWAXS images of a) **YSH-*o*F**, b) **YSH-*m*F** and c) **YSH-H**. d) Out-of-plane line cuts of the of **YSH-*o*F**, **YSH-*m*F** and **YSH-H**.

(SCLC) measurements with a hole-only device configuration of ITO/PEDOT:PSS/HTM/Al. As can be seen in Figure S32 (Supporting Information), the measured hole mobilities of **YSH-*o*F**, **YSH-*m*F**, and **YSH-H** are 8.87 × 10^{-4}, 8.34 × 10^{-4}, and 6.17 × 10^{-4} cm^2 V^{-1} s^{-1}, respectively. Notably, fluorinated HTMs exhibit relatively higher hole mobility than the non-fluorinated analogue and spiro-OMeTAD (6.52 × 10^{-4} cm^2 V^{-1} s^{-1}). This could be attributed to the enhanced dipole–dipole interactions and thus tighter intermolecular packing due to the electronegative fluorine atoms. The results are consistent with the dipole moment calculation, which indicates that **YSH-*o*F** (4.83 D) and **YSH-*m*F** (4.44 D) possess a larger dipole moment than that of **YSH-H** (1.38 D), responsible for improved hole transport ability.[11g] In order to further elucidate the effect of fluorine substitution on molecular stacking and orientation, grazing incident wide-angle X-ray scattering (GIWAXS) measurements were conducted. As shown in **Figure 3**, the **YSH-*o*F**, **YSH-*m*F** and **YSH-H** films exhibit the π–π stacking diffraction peaks along the out-of-plane direction at 1.47, 1.43, 1.39 Å^{-1}, respectively, suggesting a preferential face-on orientation. Furthermore, the d-spacing of **YSH-*o*F**, **YSH-*m*F** and **YSH-H** films are 4.42, 4.44, and 4.59 Å, respectively. The results indicate a closer molecular packing for the fluorinated HTMs, which is beneficial to hole transportation and thus higher hole mobility.

We further investigated the steady–state photoluminescence (PL) spectra and time-resolved photoluminescence (TRPL) decay measurements of perovskite film along with HTM-deposited perovskite films, which can provide charge-carrier dynamics at the interface between perovskite and HTMs. As shown in **Figure 4**a, the PL intensity of perovskites at ≈780 nm was significantly quenched when the HTMs were coated on top of the perovskite layer, compared to the pristine perovskite film. The quenching efficiency of PL emission at the interface between the perovskite and HTMs is in the order **YSH-*o*F** > **YSH-*m*F** > spiro-OMeTAD > **YSH-H**, which is in good agreement with the trend of the hole mobility values (Figure S25, Supporting Information). Compared with **YSH-H**, fluorinated HTMs showed more effective quenching of the PL emission, thereby indicating more efficient hole-extraction at the perovskite/**YSH-*o*F** and perovskite/**YSH-*m*F** interfaces. From the TRPL measurements, as illustrated in Figure 4b, and fitting with a bi-exponential decay model (I_{PL}(t) = A1 × $e^{-t/\tau 1}$ +A2 × $e^{-t/\tau 2}$),[19] the bare perovskite film showed a relatively long PL lifetime (τ) of 40.11 ns. The deposition of the HTMs on top of perovskite decreases the PL lifetime to 9.59, 13.30, 17.49, and 13.74 ns for **YSH-*o*F**, **YSH-*m*F**, **YSH-H** and spiro-OMeTAD, respectively (Table S17, Supporting Information). As a result, the perovskite film with **YSH-*o*F** on top gave the shortest lifetime, indicating the more efficient hole transfer from the perovskite to the **YSH-*o*F**. It should be noted that two fluorinated isomeric analogs (**YSH-*o*F** and **YSH-*m*F**) showed more PL emission quenching and shorter PL decay lifetime, which might be attributed to enhanced molecular packing through the dipole interaction between the molecules.[7b]

The surface morphology of the perovskite layer with and without the HTMs were studied by scanning electron microscopy (SEM) and atomic force microscope (AFM). As shown in **Figure 5**a, superior perovskite film was observed in the top-view SEM image, with organized grains in the sizes of 300–600 nm. With HTM covering the perovskite film, **YSH** series and spiro-OMeTAD blend film show smooth and completely

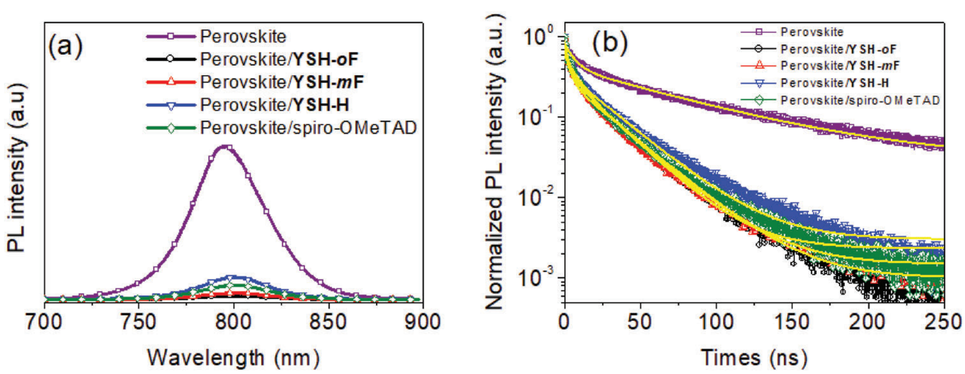

Figure 4. a) Steady–state photoluminescence spectra and b) Time-resolved photoluminescence (TRPL) spectra of different films.

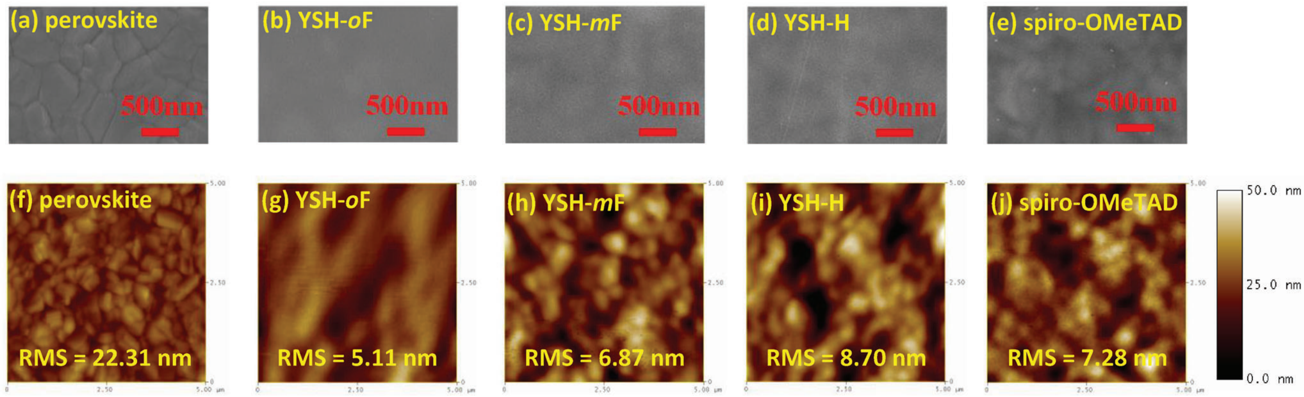

Figure 5. The top-view SEM images a–e) and AFM micrograms f–j) of perovskite film and perovskite/HTMs.

covered surface relative to pristine perovskite film. In addition, the AFM measurements show that fluorinated analogues **YSH-*o*F** and **YSH-*m*F** form more uniform films with the root-mean-square (RMS) roughness value of 5.11 and 6.87 nm, respectively compared to **YSH-H** (RMS = 8.70 nm) and spiro-OMeTAD (RMS = 7.28 nm) (Figure 5g–j). The smoother morphologies of fluorinated analogues are beneficial to hole transfer and extraction at the interface. Therefore, **YSH-*o*F** and **YSH-*m*F** are expected to result in reducing hysteresis and thus better photovoltaic efficiency.

To gain insight into the passivation effect of the **YSH** films on perovskite, X-ray photoelectron spectra (XPS) of perovskite layer with and without HTMs on it were carried out and the results are shown in **Figure 6** and Figure S33 (Supporting Information). The Pb $4f_{5/2}$ and $4f_{7/2}$ peaks of the pristine perovskite film were assigned at 143.3 and 138.5 eV, respectively. The **YSH-H**-coated perovskite film showed a slight shift of Pb 4*f* peaks toward the lower energy. In contrast, the XPS curves of the Pb $4f_{5/2}$ and $4f_{7/2}$ for perovskite/**YSH-*o*F** and perovskite/**YSH-*m*F** shifted to higher energy instead. This phenomenon has been reported to be due to the compact lattice volume and higher Fermi level of perovskites.[20] It is suggested that fluorinated HTMs may have better passivation effect than non-fluorinated one. Moreover, the XPS peaks of F 1*s* orbital for the **YSH-*o*F** and **YSH-*m*F** and S 2*p* orbital for the **YSH** series on top of perovskite layer were observed the obvious shifting of characteristic peaks. Based on the above results, we suggest that the coordination interactions between the perovskite and **YSH** HTMs may decrease the non-radiation recombination and thus improve PSCs performance. To explore the interface interaction between the **YSH** series and perovskite films, the binding energies were calculated through DFT calculations. As shown in **Figure 7**, the binding energies of −466.92 and −445.23 kcal mol^{-1}, respectively for **YSH-*o*F** and **YSH-*m*F** are higher than that of −433.79 kcal mol^{-1} for **YSH-H** without fluorine substituent, suggesting a tighter packing between the fluorinated HTMs and perovskite, resulting in more efficient interface passivation and thus more efficient hole extraction.

To evaluate the photovoltaic performance of pentafulvalene-fused HTMs, we fabricated the PSC device with the architecture of FTO/SnO_2/perovskite/HTM/Ag, while the details on device fabrication are provided in the Supporting Information. The performance of the spiro-OMeTAD-based device was measured as a reference for comparison. A mixed-halide perovskite of $Cs_{0.05}MA_{0.2}FA_{0.75}Pb(Br_{0.05}I_{0.95})_3$ as the photoactive light absorber was prepared. All the HTMs were doped with 4-*tert*-butylpyridine (*t*-BP) and lithium bis(trifluoromethanesulfonyl)imide (Li-TFSI) as additives. The cross-sectional SEM image of PSC device with **YSH-*o*F** as HTM was analyzed, as shown in **Figure 8**a, where a uniform layer of **YSH-*o*F** covered on top of perovskite with a thickness of ≈250 nm. The best current density–voltage (*J*–*V*) curves of devices with **YSH-*o*F**, **YSH-*m*F**, **YSH-H** and spiro-OMeTAD were measured under AM 1.5 G irradiation at 100 mW cm^{-2} (Figure 8b), and the corresponding photovoltaic parameters are summarized in **Table 2**. Impressively, the PSC with **YSH-*o*F** yielded the best PCE of 23.59%, with an open-circuit

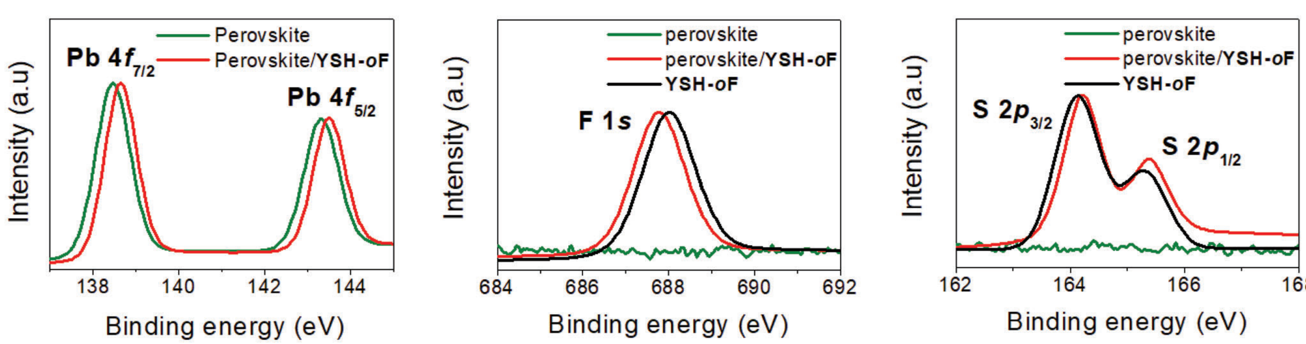

Figure 6. XPS signals of Pb 4*f*, F 1*s* and S 2*p* from a pristine **YSH-*o*F** film and a **YSH-*o*F** coated perovskite film.

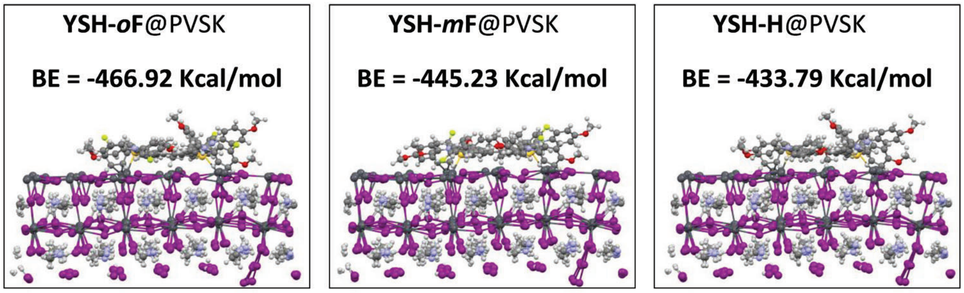

Figure 7. Binding energy (BE) of HTMs on the perovskite surface.

voltage (V_{oc}) of 1.15, a short-circuit density (J_{sc}) of 25.56 mA cm^{-2} and a fill factor (*FF*) of 80.24%. In contrast, the fluorinated isomeric analog **YSH-*m*F**-based device exhibited slightly lower PCE of 22.76%, with a V_{oc} of 1.14 V, a J_{sc} of 25.20 mA cm^{-2}, and an *FF* of 79.22%. Meanwhile, the non-fluorinated analogue **YSH-H** delivered relatively lower PCE of 20.57%, with a V_{oc} of 1.10 V, a J_{sc} of 24.27 mA cm^{-2}, and an *FF* of 77.04%. Meanwhile, the performance of fluorinated HTMs is superior to that of the spiro-OMeTAD device (22.72%). Furthermore, all the devices showed the negligible hysteresis between the forward and reverse scans (Figure S34, Supporting Information). Compared with **YSH-H**, the slightly higher V_{oc} values of fluorinated analog's devices could be attributed to the deeper HOMO energy levels observed in the DPV data, better film-forming property, and interfacial contact. Moreover, the higher FF and J_{sc} values of **YSH-*o*F** device might be ascribed to better hole-extraction ability, as verified by PL/TRPL measurements at the perovskite/**YSH-*o*F** interface, and the higher hole mobility and the better film morphology, as discussed earlier. Furthermore, the stabilized PCE were measured for 200 s, as shown in Figure 8c, and the stabilized efficiencies for **YSH** series and spiro-OMeTAD are 23.12%, 22.54%, 20.13%, and 22.42%, respectively by holding the bias of 0.96 V at the max power point. They match well with the efficiency values from *J*–*V* measurements, indicating a good reliability of the *J*–*V* curves. To further evaluate the reproducibility of the performance for **YSH** series and spiro-OMeTAD, 20 independent devices were fabricated and measured, and the efficiency histogram of the PSCs are shown in Figure 8d. The average PCEs of **YSH-*o*F**, **YSH-*m*F**, **YSH-H**, and spiro-OMeTAD were 23.31%, 22.31%, 22.28%, and 20.09%, respectively. The narrowest statistic

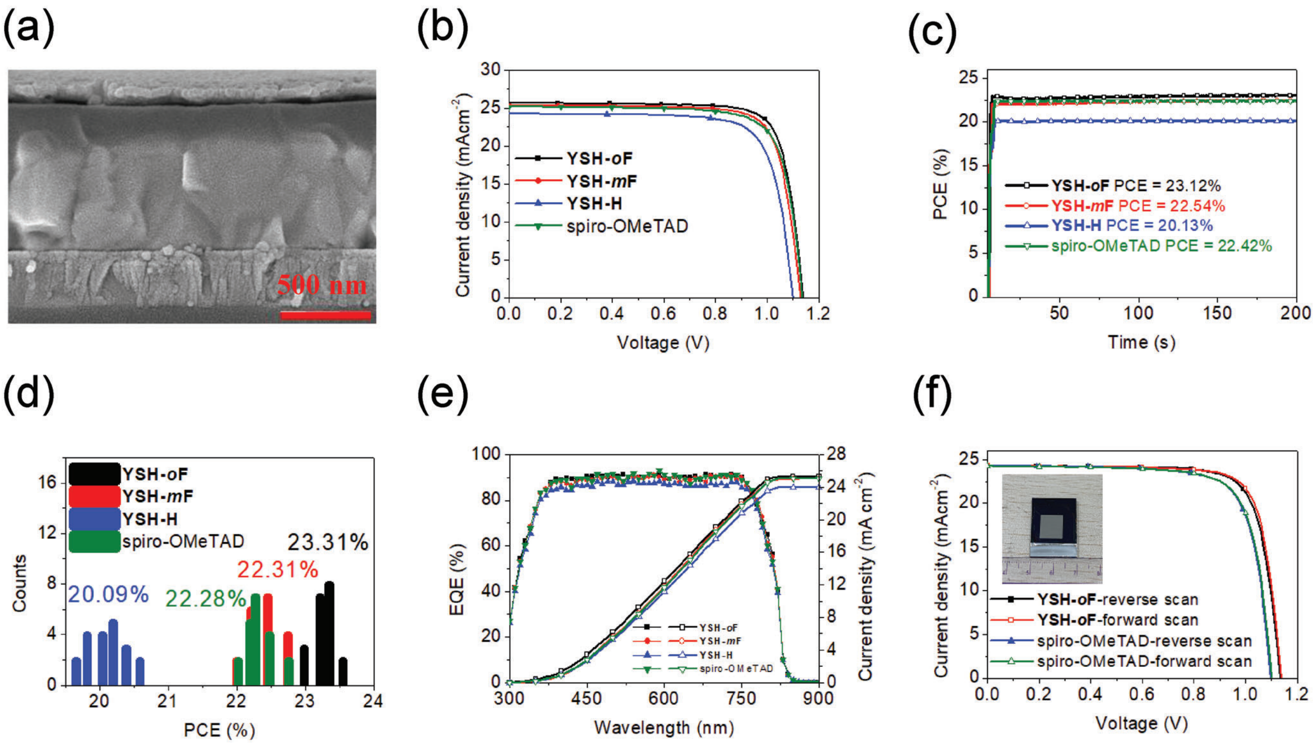

Figure 8. a) Cross-sectional SEM image of the PSC device with **YSH-*o*F** as HTM. b) *J*–*V* curves of the champion device based on **YSH** series and spiro-OMeTAD. c) Stabilized PCEs of **YSH** series and spiro-OMeTAD-based devices at maximum power point (voltage set at 0.96 V). d) Histogram of PCEs from 20 devices based on different HTMs. e) The EQE spectra and integrated current of the **YSH** series and spiro-OMeTAD-based devices. f) *J*–*V* curves of large-area PSCs (aperture area of 1.00 cm^2) based on **YSH-*o*F** and spiro-OMeTAD. Inset is a picture of the large-area PSC.

Table 2. Device parameters of the champion PSCs based on **YSH-*o*F**, **YSH-*m*F**, **YSH-H** and spiro-OMeTAD HTMs.

HTM	Scan direction		V_{oc} [V]	J_{sc} [mA cm^{-2}]	FF [%]	PCE$_{max}$ [%]
YSH-*o*F	Reverse	Best	1.15	25.56	80.24	23.59
	Reverse	Average	1.14 ± 0.012	25.52 ± 0.008	80.11 ± 0.11	23.31 ± 0.09
	Forward		1.14	25.67	80.01	23.41
YSH-*m*F	Reverse	Best	1.14	25.20	79.22	22.76
	Reverse	Average	1.12 ± 0.011	25.08 ± 0.07	78.03 ± 0.60	22.31 ± 0.48
	Forward		1.14	25.18	77.78	22.32
YSH-H	Reverse	Best	1.10	24.27	77.04	20.57
	Reverse	Average	1.09 ± 0.008	23.94 ± 0.30	76.98 ± 0.04	20.09 ± 0.25
	Forward		1.10	24.26	76.63	20.45
Spiro-OMeTAD	Reverse	Best	1.13	25.36	79.30	22.72
	Reverse	Average	1.12 ± 0.007	25.11 ± 0.19	79.22 ± 0.06	22.28 ± 0.16
	Forward		1.13	25.40	78.87	22.63

distribution of PCE value is achieved for **YSH-*o*F**, possibly resulting from the quality of HTM film deposited on top of perovskite (Figure 5). In view of the high charge mobility, the potential of **YSH** series as dopant-free HTMs was evaluated by fabricating the PSCs. As shown in Figure S35 and Table S18 (Supporting Information), the **YSH-*o*F**, **YSH-*m*F**, **YSH-H**, and spiro-OMeTAD-based devices showed significantly lower efficiency values, which reached the PCEs of 12.38%, 11.28%, 8.17%, and 9.75%, respectively under reverse scan as a consequence of the reduced V_{oc}, J_{sc}, and FF. Thus, the dopant is of help in current case.

The corresponding external quantum efficiency (EQE) spectra and integrated current density (integrated J_{sc}) of **YSH-*o*F**, **YSH-*m*F**, **YSH-H**, and spiro-OMeTAD-based devices were recorded in Figure 8e. The integrated J_{sc} values calculated from EQE curves with **YSH-*o*F**, **YSH-*m*F**, **YSH-H**, and spiro-OMeTAD layers were 25.32, 25.03, 23.95, and 25.11 mA cm^{-2}, respectively, which were in accordance with the J_{sc} values from *J*–*V* curves. To test the potential for practical application, we fabricated large-area PSCs with an active area of 1.00 cm^2 based on **YSH-*o*F**. As illustrated in Figure 8f, the optimized device efficiency for **YSH-*o*F** gave a PCE of 21.92%, with a V_{oc} of 1.14 V, a J_{sc} of 24.30 mA cm^{-2}, and an *FF* of 79.14%, which is higher than the maximum value of 18.63% for the spiro-OMeTAD-based device. It might be attributed to the better film quality for the former HTM.

In addition to the performance in terms of efficiency, the long-term durability of unencapsulated PSCs based on **YSH** series and spiro-OMeTAD was also evaluated at room temperature with 40% humidity and the thermal stability monitored at 85 °C in glove box. As shown in **Figure 9**, the fluorinated analogues **YSH-*o*F**- and **YSH-*m*F**-based devices showed better stability, with 88% and 86% of the initial PCE retained after 1000 h storage at room temperature, respectively, while the non-fluorinated analogues **YSH-H** retained 81% of the initial efficiency. In contrast, the device based on spiro-OMeTAD exhibited inferior stability, with only 71% of the original PCE. The better stability of devices with **YSH-*o*F** and **YSH-*m*F** than **YSH-H** could be attributed to the better hydrophobicity of the films. As shown in Figure S36 (Supporting Information), the water-contact angles of **YSH-*o*F** (81°) and **YSH-*m*F** (79°) are higher than that of **YSH-H** (76°) and spiro-OMeTAD (73°), presumably due to the incorporation of fluorine atoms in **YSH-*o*F** and **YSH-*m*F**. Thus, fluorinated HTMs can effectively prevent the perovskite layer from the penetration of moisture, which is beneficial to enhancing the long-term stability of PSCs. Furthermore, the enhanced stability of fluorinated HTMs **YSH-*o*F**- and **YSH-*m*F**-based PSCs might be ascribed to their low-lying HOMO energy levels.[21] Under high temperature conditions (85 °C) in nitrogen and dark environment, the PSCs employed **YSH-*o*F**, **YSH-*m*F**, and **YSH-H** retained 84%, 81%, and 76% of their original PCEs after 500 h. However, the

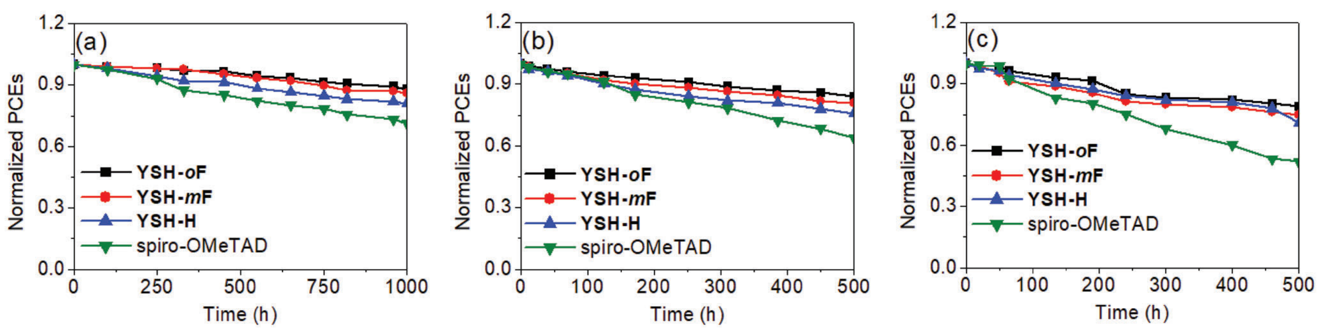

Figure 9. Normalized long-term device stability of **YSH-*o*F**-, **YSH-*m*F**-, **YSH-H**- and spiro-OMeTAD-based PSCs: a) stored at 20–25 °C environment; b) thermal stressed at 85 °C; and c) continuous light soaking (100 mW cm^{-2}) in glovebox (N_2 atmosphere;H_2O :0.1 ppm;O_2:0.5 ppm) at 40 °C.

PSC with spiro-OMeTAD maintained 64% of its initial efficiency after 500 h. Furthermore, we measured the stability of the **YSH-*o*F**-, **YSH-*m*F**-, **YSH-H-** and spiro-OMeTAD-based devices under continuous light irradiation in a glovebox (N_2 atmosphere;H_2O :0.1 ppm;O_2:0.5 ppm) at 40 °C. It was observed that the devices based on **YSH-*o*F** and **YSH-*m*F** exhibited great stability and over 70% of their original PCEs could be maintained after 500 h. The better photostability of the **YSH-*o*F**- and **YSH-*m*F**-based PSCs could be ascribed to the better HTM film morphology, leading to favorable interfacial contact between the perovskite layer and HTM, which could protect the perovskite film from moisture penetration, and thus improved long term stability of devices.

3. Conclusion

In this work, a series of novel 2D pentafulvalene-fused derivatives with extended π-conjugation system, i.e., **YSH-*o*F**, **YSH-*m*F** and **YSH-H**, were designed and successfully utilized as hole-transport layer in fabricating high-performance PSCs. Planarity of π-conjugated framework of the DCPDT motif effectively facilitates intermolecular π–π packing interactions, thus leading to improved hole mobility and enhanced PCE. Compared to non-fluorinated **YSH-H**, the fluorinated analogues **YSH-*o*F** and **YSH-*m*F** exhibited more favorable energy-level alignment due to strong electron-withdrawing fluorine substituents on HTMs, leading to a down-shifted HOMO energy level, which increases the V_{oc} values and thus PCEs. In addition, the fluorinated analogues **YSH-*o*F** and **YSH-*m*F** exhibited better hole-extraction efficiency and reduced non-radiative recombination at the perovskite/HTM interface as indicated by PL/TRPL and SCLC results. Moreover, **YSH-*o*F** and **YSH-*m*F** showed a tight contact with perovskite films according to and the DFT calculation, leading to improved interfacial passivation and thus afford a better PSC. Furthermore, fluorinated HTM **YSH-*o*F** and **YSH-*m*F** can boost the intermolecular stacking relative to the non-fluorinated counterpart **YSH-H**, as verified by GIWAXS measurement. This might be attributed to a stronger dipole–dipole interaction between the molecules. As a result, an excellent PCE of 23.59% and 22.76%, respectively, was achieved with **YSH-*o*F** and **YSH-*m*F** for small-area (0.09 cm^2) PSCs, superior to that from **YSH-H** counterpart (20.57%). Moreover, the **YSH-*o*F**-based devices exhibit a superior PCE of 21.92% for large-area (1.00 cm^2) PSCs. Meanwhile, with the fluorinated **YSH-*o*F** and **YSH-*m*F** as HTMs, significantly improved long-term stability was obtained compared with **YSH-H** and spiro-OMeTAD without encapsulation under various aging conditions, presumably due to the hydrophobicity of the fluorinated HTMs. Over 80% of their initial PCEs was retained after more than 1000 h ambient exposure, or over 75% of the initial PCE was retained after aging at 85 °C for 500 h. Alternatively, over 70% of the initial PCE after 500 h continuous light illumination. Our results demonstrate that the pentafulvalene-fused organic small molecules are potential candidates as HTMs for achieving high-performance PSCs.

Supporting Information

Supporting Information is available from the Wiley Online Library or from the author.

Acknowledgements

Y.-D.L. thanks the support from Ministry of Science and Technology, Taiwan (Grant Number MOST 111-2628-M-031-001-MY3). K.-M.L. thanks the support from Ministry of Science and Technology, Taiwan (Grant Number MOST 111-2223-E-182-001-MY4), Chang Gung University (QZRPD181) and Chang Gung Memorial Hospital, Linkou, Taiwan (CMRPD2M0042). The authors are grateful to the National Center for High-performance Computing for computer time and facilities.

Conflict of Interest

The authors declare no conflict of interest.

Data Availability Statement

The data that support the findings of this study are available in the supplementary material of this article.

Keywords

fluorine-substituted small molecules, hole-transporting materials, long-term stability, pentafulvalene-fused derivatives, perovskite solar cells

Received: June 6, 2023
Revised: July 11, 2023
Published online:

[1] a) A. Kojima, K. Teshima, Y. Shirai, T. Miyasaka, *J. Am. Chem. Soc.* **2009**, *131*, 6050; b) Y. Jiang, S. He, L. Qiu, Y. Zhao, Y. Qi, *Appl. Phys. Rev.* **2022**, *9*, 021305; c) R. Lin, J. Xu, M. Wei, Y. Wang, Z. Qin, Z. Liu, J. Wu, K. Xiao, B. Chen, S. M. Park, G. Chen, H. R. Atapattu, K. R. Graham, J. Xu, J. Zhu, L. Li, C. Zhang, E. H. Sargent, H. Tan, *Nature* **2022**, *603*, 73; d) M. Jeong, I. W. Choi, E. M. Go, Y. Cho, M. Kim, B. Lee, S. Jeong, Y. Jo, H. W. Choi, J. Lee, J.-H. Bae, S. K. Kwak, D. S. Kim, C. Yang, *Science* **2020**, *369*, 1615.

[2] NREL, Best Research-Cell Efficiencies (https://www.nrel.gov/pv/cell-efficiency.html%20(accessed:%20April%202023) (accessed: May 2023).

[3] a) Y. Zhao, F. Ma, Z. Qu, S. Yu, T. Shen, H.-X. Deng, X. Chu, X. Peng, Y. Yuan, X. Zhang, J. You, *Science* **2022**, *377*, 531; b) T. Niu, W. Zhu, Y. Zhang, Q. Xue, X. Jiao, Z. Wang, Y.-M. Xie, P. Li, R. Chen, F. Huang, Y. Li, H.-L. Yip, Y. Cao, *Joule* **2021**, *5*, 249; c) D.-J. Xue, Y. Hou, S.-C. Liu, M. Wei, B. Chen, Z. Huang, Z. Li, B. Sun, A. H. Proppe, Y. Dong, M. I. Saidaminov, S. O. Kelley, J.-S. Hu, E. H. Sargent, *Nat. Commun.* **2020**, *11*, 1514.

[4] a) T. Zhang, F. Wang, H.-B. Kim, I.-W. Choi, C. Wang, E. Cho, R. Konefal, Y. Puttisong, K. Terado, L. Kobera, M. Chen, M. Yang, S. Bai, B. Yang, J. Suo, S.-C. Yang, X. Liu, F. Fu, H. Yoshida, W. M. Chen, J. Brus, V. Coropceanu, A. Hagfeldt, J.-L. Bredas, M. Fahlman, D. S. Kim, Z. Hu, F. Gao, *Science* **2022**, *377*, 495; b) J.-Y. Seo, S. Akin, M. Zalibera, M. A. R. Preciado, H.-S. Kim, S. M. Zakeeruddin, J. V. Millc, M. Grätzel, *Adv. Funct. Mater.* **2021**, *31*, 2102124; c) J. Feng, Y. Jiao, H. Wang, X. Zhu, Y. Sun, M. Du, Y. Cao, D. Yang, S. F. Liu, *Energy Environ. Sci.* **2021**, *14*, 3035; d) J. Siekmann, S. Ravishankar, T. Kirchartz, *ACS Energy Lett.* **2021**, *6*, 3244.

[5] a) F. Fabregat-Santiago, J. Bisquert, L. Cevey, P. Chen, M. Wang, S. M. Zakeeruddin, M. Grätzel, *J. Am. Chem. Soc.* **2009**, *131*, 558; b) J. Liu, Y. Wu, C. Qin, X. Yang, T. Yasuda, A. Islam, K. Zhang, W. Peng, W. Chen, L. Han, *Energy Environ. Sci.* **2014**, *7*, 2963; c) J. Kong, Y. Shin,

J. A. Rohr, H. Wang, J. Meng, Y. Wu, A. Katzenberg, G. Kim, D. Y. Kim, T.-D. Li, E. Chau, F. Antonio, T. Siboonruang, S. Kwon, K. Lee, J. R. Kim, M. A. Modestino, H. Wang, A. D. Taylor, *Nature* **2021**, *594*, 51.

[6] a) Z. A. Li, Z. L. Zhu, C. C. Chueh, S. B. Jo, J. D. Luo, S. H. Jang, A. K. Y. Jen, *J. Am. Chem. Soc.* **2016**, *138*, 11833; b) P. Xu, P. Liu, Y. Li, B. Xu, L. Kloo, L. Sun, Y. Hua, *ACS Appl. Mater. Interfaces* **2018**, *10*, 19697; c) H. Zhang, Y. Wu, W. Zhang, E. Li, C. Shen, H. Jiang, H. Tian, W.-H. Zhu, *Chem. Sci.* **2018**, *9*, 5919; d) S. A. Ok, B. Jo, S. Somasundaram, H. J. Woo, D. W. Lee, Z. Li, B. G. Kim, J. H. Kim, Y. J. Song, T. K. Ahn, S. Park, H. J. Park, *Nat. Commun.* **2018**, *9*, 4537.

[7] a) Z. Li, Y. Tong, J. Ren, Q. Sun, Y. Tian, Y. Cui, H. Wang, Y. Hao, C.-S. Lee, *Chem. Eng. J.* **2020**, *402*, 125923; b) J. Ren, J. Qu, J. Chen, Z. Li, Q. Sun, H. Wang, Z. Yu, Y. Hao, *J. Power Sources* **2018**, *401*, 29.

[8] a) I. Cho, N. J. Jeon, O. K. Kwon, D. W. Kim, E. H. Jung, J. H. Noh, J. Seo, S. I. Seok, S. Y. Park, *Chem. Sci.* **2017**, *8*, 734; b) K. Liu, S. Dai, F. Meng, J. Shi, Y. Li, J. Wu, Q. Meng, X. Zhan, *J. Mater. Chem. A* **2017**, *5*, 21414; c) F. Wu, Y. Ji, C. Zhong, Y. Liu, L. X. Tan, L. N. Zhu, *Chem. Commun.* **2017**, *53*, 8719; d) B. Wang, H. Wang, G. Sathiyan, C. Chen, Y. Xu, M. Cheng, *ACS Appl. Energy Mater.* **2022**, *5*, 5901.

[9] a) A. Molina-Ontoria, I. Zimmermann, I. Garcia-Benito, P. Gratia, C. Roldan-Carmona, S. Aghazada, M. Grätzel, M. K. Nazeeruddin, N. Martin, *Angew. Chem., Int. Ed.* **2016**, *128*, 6378; b) K. Strakova, L. Assies, A. Goujon, F. Piazzolla, H. V. Humeniuk, S. Matile, *Chem. Rev.* **2019**, *119*, 10977; c) K. Yang, Q. Liao, J. Huang, Z. Zhang, M. Su, Z. Chen, Z. Wu, D. Wang, Z. Lai, H. Y. Woo, Y. Cao, P. Gao, X. Guo, *Angew. Chem., Int. Ed.* **2022**, *134*, e202113749; d) X. Li, S. Wang, G. Xu, S. Liu, Y. Li, Y. Li, *Adv. Funct. Mater.* **2021**, *21*, 20106906; e) S. Venkateswarlu, Y.-D. Lin, K.-M. Lee, K.-L. Liau, Y. T. Tao, *ACS Appl. Mater. Interfaces* **2020**, *12*, 50495; f) Y. Wang, W. Chen, L. Wang, B. Tu, T. Chen, B. Liu, K. Yang, C. W. Koh, X. Zhang, H. Sun, G. Chen, X. Feng, H. Y. Woo, A. B. Djurišić, Z. He, X. Guo, *Adv Mater* **2019**, *31*, 1902781.

[10] a) M. Saliba, S. Orlandi, T. Matsui, S. Aghazada, M. Cavazzini, J.-P. Correa-Baena, P. Gao, R. Scopelliti, E. Mosconi, K.-H. Dahmen, F. De Angelis, A. Abate, A. Hagfeldt, G. Pozzi, M. Grätzel, M. K. Nazeeruddin, *Nat. Energy* **2016**, *1*, 5017; b) M. Franckevicius, A. Mishra, F. Kreuzer, J. Luo, S. M. Zakeeruddin, M. Grätzel, *Mater Horiz* **2015**, *2*, 613; c) S. Ma, H. Zhang, N. Zhao, Y. Cheng, M. Wang, Y. Shen, G. Tu, *J. Mater. Chem. A* **2015**, *3*, 12139.

[11] a) Y.-D. Lin, K.-M. Lee, B.-Y. Ke, K.-S. Chen, H.-C. Cheng, W.-J. Lin, S. H. Chang, C.-G. Wu, M.-C. Kuo, H.-C. Chung, C.-C. Chou, H.-Y. Chen, K.-L. Liau, T. J. Chow, S.-S. Sun, *Energy Technol.* **2019**, *7*, 307; b) Y.-D. Lin, S. Y. Abate, H.-C. Chung, K.-L. Liau, Y.-T. Tao, T. J. Chow, S.-S. Sun, *ACS Appl. Energy Mater.* **2019**, *2*, 7070; c) K.-M. Lee, K.-S. Chen, J.-R. Wu, Y.-D. Lin, S.-M. Yu, S. H. Chang, *Nanoscale* **2018**, *10*, 17699; d) Y.-D. Lin, K.-M. Lee, S. H. Chang, T.-Y. Tsai, H.-C. Chung, C.-C. Chou, H.-Y. Chen, T. J. Chow, *ACS Appl. Energy Mater.* **2021**, *4*, 4719; e) K.-M. Lee, W.-H. Chiu, Y.-H. Tsai, C.-S. Wang, Y. T. Tao, Y.-D. Lin, *Chem. Eng. J.* **2022**, *407*, 131609; f) K.-M. Lee, J.-Y. Yang, P.-S. Lai, K.-J. Luo, T.-Y. Yang, K.-L. Liau, S. Y. Abate, Y.-D. Lin, *Chem. Commun.* **2021**, *57*, 6444; g) K.-M. Lee, S. Y. Abate, J. H. Yang, W.-H. Chiu, S. Ahn, S.-R. Li, K.-L. Liau, Y. T. Tao, Y.-D. Lin, *Chem. Eng. J.* **2023**, *454*, 139926.

[12] J. Wu, W. Pisula, K. Müllen, *Chem. Rev.* **2007**, *107*, 718.

[13] a) F. G. Brunetti, X. Gong, M. Tong, A. J. Heeger, F, W., *Angew. Chem.* **2010**, *122*, 542; b) K. Loganathan, E. G. Cammisa, B. D. Myron, P. G. Pickup, *Chem. Mater.* **2003**, *15*, 1918; c) K. Loganathan, P. G. Pickup, *Electrochim. Acta* **2005**, *51*, 41.

[14] J. Luo, K.-W. Huang, H. Qu, X. Zhang, L. Zhu, H. S. O. Chan, C. Chi, *Org. Lett.* **2010**, *12*, 5660.

[15] K. Rakstys, M. Saliba, P. Gao, P. Gratia, E. Kamarauskas, S. Paek, V. Jankauskas, M. K. Nazeeruddin, *Angew. Chem., Int. Ed.* **2016**, *55*, 7464.

[16] a) R. Grisorio, B. Roose, S. Colella, A. Listorti, G. P. Suranna, A. Abate, *ACS Energy Lett.* **2017**, *2*, 1029; b) Q. Wang, E. Mosconi, C. Wolff, J. Li, D. Neher, F. De Angelis, G. P. Suranna, R. Grisorio, A. Abate, *Adv. Energy Mater.* **2019**, *9*, 1900990.

[17] J. Luo, K.-W. Huang, H. Qu, X. Zhang, L. Zhu, H. S. O. Chan, C. Chi, *Org. Lett.* **2010**, *12*, 5660.

[18] a) H. D. Pham, T. T. Do, J. Kim, C. Charbonneau, S. Manzhos, K. Feron, W. C. Tsoi, J. R. Durrant, S. M. Jain, P. Sonar, *Adv. Energy Mater.* **2018**, *8*, 1703007; b) Y. He, N. Li, T. Heumüller, J. Wortmann, B. Hanisch, A. Aubele, S. Lucas, G. Feng, X. Jiang, W. Li, P. B¨auerle, C. J. Brabec, *Joule* **2022**, *6*, 1160.

[19] Y. Lin, L. Shen, J. Dai, Y. Deng, Y. Wu, Y. Bai, X. Zheng, J. Wang, Y. Fang, H. Wei, W. Ma, X. C. Zeng, X. Zhan, J. Huang, *Adv. Mater.* **2017**, *29*, 1604545.

[20] a) H. Zhao, Y. Han, Z. Xu, C. Duan, S. Yang, S. Yuan, Z. Yang, Z. Liu, S. Liu, *Adv. Energy Mater.* **2019**, *9*, 1902279; b) R. Prasanna, T. Leijtens, S. P. Dunfield, J. A. Raiford, E. J. Wolf, S. A. Swifter, J. Werner, G. E. Eperon, C. de Paula, A. F. Palmstrom, C. C. Boyd, M. F. A. M. van Hest, S. F. Bent, G. Teeter, J. J. Berry, M. D. McGehee, *Nat. Energy* **2019**, *4*, 939; c) X. Yu, D. Gao, Z. Li, X. Sun, B. Li, Z. Zhu, Z. Li, *Angew. Chem., Int. Ed.* **2023**, *62*, e202218752; d) Z. Zhang, L. Shen, S. Wang, L. Zheng, D. Li, Z. Li, Y. Xing, K. Guo, L. Xie, Z, W., *Adv. Energy Mater.* **2023**, *13*, 2204362.

[21] L. Huo, Y. Zhou, Y. Li, *Rapid Commun.* **2009**, *30*, 925.